

# Pleistocene stratigraphy and paleoenvironmental variation from Lomonosov Ridge sediments, central Arctic Ocean

M. Jakobsson<sup>a,\*</sup>, R. Løvlie<sup>b</sup>, E.M. Arnold<sup>a</sup>, J. Backman<sup>a</sup>, L. Polyak<sup>c</sup>,  
J.-O. Knutsen<sup>b</sup>, E. Musatov<sup>d</sup>

<sup>a</sup> Department of Geology and Geochemistry, Stockholm University, S-106 91 Stockholm, Sweden

<sup>b</sup> Institute of Solid Earth Physics, Allégt. 41, N-5007, Bergen, Norway

<sup>c</sup> Byrd Polar Research Center, Ohio State University, Columbus, OH 43210, USA

<sup>d</sup> VNIIOkeangeologia, 1st Angliysky Ave., 190121 St. Petersburg, Russian Federation

Received 28 December 1999; accepted 23 May 2000

---

## Abstract

High resolution seismoacoustic chirp sonar data and piston cores were collected from the Lomonosov Ridge in the central Arctic Ocean (85°–90°N; 130°–155°E). The chirp sonar data indicate substantial erosion on the ridge crest above 1000 mbsl while data from deeper sites show apparently undisturbed sedimentation. Piston cores from both the eroded ridge crest and the slopes have been analyzed for a variety of properties, permitting inter-core correlation and description of paleoenvironmental change over time. Based on the evidence of extensive sediment erosion at depths above 1000 mbsl, we infer that the top of the Lomonosov Ridge has been eroded by grounded ice during a prominent glacial event that took place during MIS 6 according to a newly published age model. This event is coeval with a dramatic shift from low amplitude glacial–interglacial variability to high amplitude variability recorded in the sedimentary record. The new age model used in our study is based on nanofossil biostratigraphy and correlation between sedimentary cycles and a low-latitude oxygen isotope record and confirmed by paleomagnetic polarity studies where negative paleomagnetic inclinations are assigned to excursions. Due to the controversy between this age model and age models that assign the negative paleomagnetic inclinations to polarity reversals, we provide a correlation to Lomonosov Ridge core PS2185-6 [Spielhagen et al., *Geology*, 25 (1997) 783]. According to the latter age models, the Lomonosov Ridge was eroded by ice grounding much earlier, at MIS 16. © 2001 Elsevier Science B.V. All rights reserved.

*Keywords:* Arctic Ocean; grain size; magnetics; seismics; sediment erosion; ice grounding; nanofossils; foraminiferas; stratigraphy

---

## 1. Introduction

The Arctic Ocean perennial ice cover is primarily comprised of sea ice and smaller amounts of glacial ice. The primary sediment transport mechanism from the surrounding land and shallow shelf areas to the central Arctic Ocean ridges takes place by incorpora-

---

\* Corresponding author. Current address: Center for Coastal and Ocean Mapping, University of New Hampshire, 24 Colovos Road, Durham, NH 03824, USA. Tel.: +1-603-862-3755.

E-mail address: martin.jakobsson@unh.edu (M. Jakobsson).

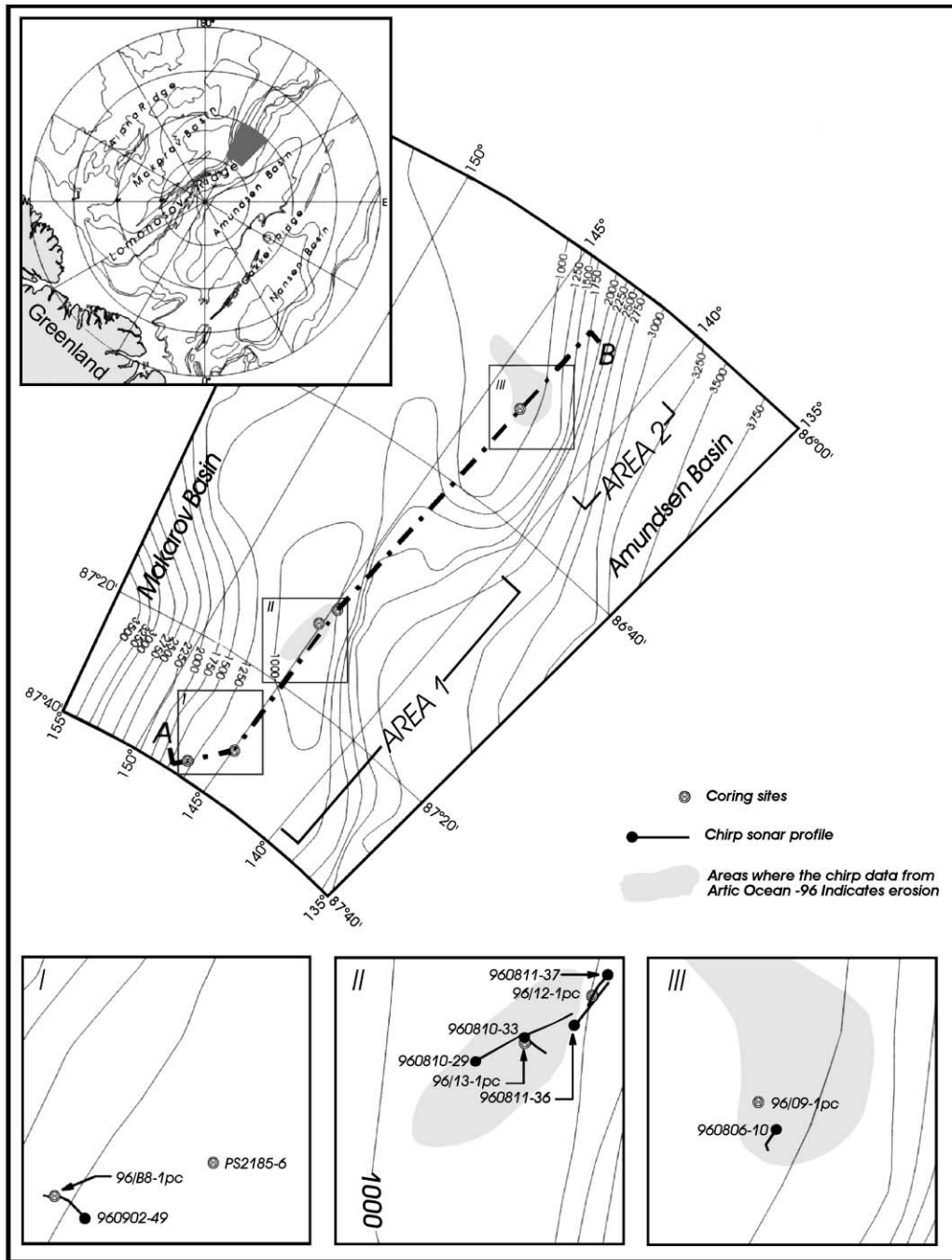


Fig. 1. Location map of the study area on the Lomonosov Ridge crest. The dotted line between A and B indicates the bathymetric profile shown in Fig. 2.

tion of sediment into these two types of ice (Clark and Hansen, 1983), in contrast to the deep basins where turbidity currents act as the major transport mechanism (e.g., Stein and Korolev, 1994). The modern shallow shelf areas, covering about 36% of the entire Arctic Ocean (Carmack, 1990), represent highly dynamic environments through the Pleistocene due to large variations in sea level, river discharge (e.g., Stein, 1998) and the formation and decay of major ice sheets (e.g., Larsen et al., 1999; Dyke, 1999). Given that sedimentation on the central Arctic Ocean ridges is essentially the product of glacial and sea ice activity at present, these sediments preserve records of the onset and dynamic evolution of the major northern hemisphere ice sheets and the Arctic Ocean perennial sea ice cover.

During the summer of 1996, the Swedish Polar Secretariat organized an expedition to the central Arctic (*Arctic Ocean-96*), aboard the icebreaker *Oden*. The sampling program included conventional piston and gravity coring, as well as seismoacoustic data acquisition. In this study, we present multidisciplinary work focused on studies of four cores collected from a North–South transect along the Lomonosov Ridge crest (Fig. 1, Table 1). Several data sets have been generated, including high-resolution acoustic stratigraphy (Jakobsson, 1999), lithostratigraphy, sediment physical properties (GRAPE density, p-wave velocity and shear strength), magnetic properties (NRM, susceptibility, rock magnetic parameters, magnetic fabric), grain size and calcareous nannofossil biostratigraphy. The major purposes of this research are to use a newly derived chronology for the Lomonosov Ridge sediments (Jakobsson et al., 2000) to (1) study glacial–interglacial variability, (2) reconstruct the paleoceanographic history of the central Arctic Ocean, (3) provide core/seismic

integration, and (4) correlate our Lomonosov Ridge cores with other sediment cores from the region (Fütterer, 1992; Spielhagen et al., 1997).

The high-resolution acoustic stratigraphy from Jakobsson (1999) shows evidence for substantial erosion on the crest of the Lomonosov Ridge down to ca. 1000 m water depth. Ice grounding and/or currents were suggested as the most likely causes of this erosion. However, a conclusive interpretation could not be made from the *Arctic Ocean-96* expedition seismoacoustic records. During the summer of 1999, the US Nuclear submarine, *USS Hawkbill*, collected acoustic data under the auspices of the SCICEX program using a sidescan swath bathymetric sonar and a chirp sonar. The SCICEX data indicate glacial fluting and scouring of seafloor and large-scale glacial erosion on the crest of the Lomonosov Ridge (Polyak et al., 2001). The cores we include in this study are located on both the eroded shallow crest of the ridge as well as the non-eroded deeper parts as indicated by our high-resolution chirp sonar data over the coring sites. Through core/seismic integration and inter-core correlation, we are able to constrain the stratigraphic position of the major erosional phase in the sector between 85°20' N and 87°40' N of the Lomonosov Ridge.

## 2. Stratigraphy of the Lomonosov Ridge sediment

### 2.1. Acoustic stratigraphy

The stratigraphy of the Lomonosov Ridge sediments, derived from multichannel seismic reflection data, has been described by Jokat et al. (1992, 1995). They subdivided the upper 2 km of the ridge sequence into six seismic units (LR1–LR6). The upper-

Table 1  
Core locations and distance to nearest chirp sonar record

Core	Location	Water depth (m)	Recovery (cm)	Distance to chirp record (m)
96/B8-1pc	146°52'58"E, 87°37'18"N	1261	645	60
96/13-1pc	145°10'08"E, 87°09'12"N	978	456	260
96/12-1pc	144°46'22"E, 87°05'51"N	1003	722	50
96/09-1pc	143°26'37"E, 86°24'52"N	927	270	2700
PS2185-6 <sup>a</sup>	144°55'36"E, 87°32'12"N	1052	768	–

<sup>a</sup>Spielhagen et al., 1997.

most ca. 500 m of this sequence consists of flat lying strata which accumulated after the ridge subsided below sea level about 50 Ma (Jokat et al., 1995). A prominent unconformity below these flat lying sediments was likely formed from sub-aerial and shallow marine erosion that occurred during ridge subsidence below sea level (Jokat et al., 1995).

The sedimentary sequence within Unit LR6 (uppermost 80–100 m) has been studied by high-resolution seismic surveying methods (Blasco et al., 1979; Fütterer, 1992; Jakobsson, 1999). The areas of the Lomonosov Ridge where the high-resolution chirp sonar data from the *Arctic Ocean-96* expedition indicate substantial erosion are shown in Fig. 1. Estimates based on these seismoacoustic data suggest that more than 50 m of the sediment section is missing in the shallowest areas of the ridge crest. The erosion was observed only in water depths shallower than approximately 1000 m; in the deeper surveyed areas, the chirp profiles indicate conformable, acoustically well-stratified sequences. The acoustic stratigraphy within Unit LR6 has been subdivided into five seismoacoustic units bounded by prominent reflectors in the chirp records (Jakobsson, 1999). The uppermost Unit 5 (~4 ms TWT) consists of sediments deposited after a major erosional phase. The erosional surface occurs as an angular unconformity as well as a disconformity. Unit 5 is thus bounded by the sea-floor and a prominent reflector, reflector A, which defines the end of the major erosional event. A semi-transparent to transparent unit (Unit 4) is present in conjunction with some areas of erosion and was interpreted to consist of reworked material (Jakobsson, 1999).

## 2.2. Sediment stratigraphy

Arctic Ocean sediments have been extensively studied, and many investigators have recognized glacial–interglacial variability in sediment texture, chemistry, color and faunal assemblages (e.g., Phillips and Grantz, 1997; Spielhagen et al., 1997; Jones et al., 1999). A widely applied standard lithostratigraphy was developed by Clark et al. (1980), which has provided a common stratigraphic framework for investigators to correlate sediments across vast areas of the Arctic Ocean.

While this common stratigraphic framework and cyclical glacial/interglacial variability is widely recognized in the Arctic Ocean, precise dating of the sediments has largely relied upon magnetic reversal stratigraphy due to the dearth of diagnostic microfossils (Steuerwald et al., 1968; Clark, 1970). Cores raised from Ice Island T-3 in the Canadian Arctic during the 1960s yielded polarity stratigraphies that were presumed to extend into the Gauss (2.6 Ma) and Gilbert (3.57 Ma) Chrons, suggesting sedimentation rates on the order of mm/ka (Steuerwald et al., 1968; Clark, 1970). These low sedimentation rates were challenged by both amino acid epimerization studies (Sejrup et al., 1984) and paleomagnetic investigations. The latter attributed negative paleomagnetic inclinations to magnetic excursions rather than to polarity reversals (Løvlie et al., 1986). Recent investigations of 25 cores from the Fram Strait, Yermak Plateau and the Nansen-Gakkel Ridge confirmed the presence of magnetic excursions within the Brunhes Chron (0–0.78 Ma) (Nowaczyk and Baumann, 1992), implying relatively high sedimentation rates in these sections of the Arctic Ocean. Nannofossil biostratigraphy from these cores and from the Lomonosov Ridge (Gard, 1993) suggested sedimentation rates on the order of cm/ka, comparable to those in temperate oceans. Based mainly on AMS  $^{14}\text{C}$  dating, sedimentation rates in eastern central Arctic Ocean box cores have been suggested to range between 0.4 and >2cm/ka during MIS 1 and 0.4 and 0.9 cm/ka during MIS 2 (Stein et al., 1994b).

Here, we will apply a new age model to the Lomonosov Ridge sediments which is based on paleomagnetic stratigraphy and glacial/interglacial variations in sediment chemistry, color and biostratigraphy. This age model is derived from detailed studies of core 96/12-1pc, which exhibits variations in manganese content and color, mimicking low-latitude  $\delta^{18}\text{O}$  glacial/interglacial cyclicity (Jakobsson et al., 2000). The combined Mn and color cyclicity provides stratigraphic information that together with biostratigraphic data permits the construction of a detailed chronological model. Correlation of the resulting age model to established age estimates of geomagnetic excursions in the Brunhes Chron reveals a remarkable fit between the two independently derived time scales. Due to the incompatibility of our

age model and age models that assign negative paleomagnetic inclinations to polarity reversals, we also provide a stratigraphic correlation to Lomonosov Ridge core PS2185-6 (Spielhagen et al., 1997) so that the two age models can be directly compared.

### 3. Data collection and methods

A detailed description of the methods can be found in the electronic appendix.<sup>1</sup> High-resolution seismoacoustic data were acquired on *Oden* with an X-Star chirp sonar system used with a SC-512 tow fish. Surveying was mainly performed with a 2–4-kHz 100-ms-long chirp pulse, resulting in a sediment penetration between about 40 and 90 ms TWT with a resolution of approximately 1 ms TWT in water depths ranging between about 600 and 2500 m.

A total of 24 piston cores were raised from the Lomonosov Ridge area during the *Arctic Ocean-96* expedition. The core processing was initiated with measurements of GRAPE density, p-wave velocity and magnetic susceptibility at 1-cm intervals using a whole core Multi Sensor Track (MST) at the Bedford Institute of Oceanography, Halifax. Sediment lithology was visually described prior to destructive measurements and sampling. Undrained shear strength measurements were conducted on the split core's working half with a motorized vane shear device and with a hand-held penetrometer for highly consolidated intervals. In core 96/09-1pc, a one-dimensional consolidation test was performed with an odometer using incremented loading steps.

Samples for discrete magnetic measurements were retrieved by continuous sampling with thin-walled cubic plastic boxes (6.2 cm<sup>3</sup>). The bottom 3 m of core 96/12-1pc was sampled with two 1.5-m-long U-channels (2 × 2 cm). Paleomagnetic measurements of these U-channels were performed in Gif-sur-Yvette using a 2G DC SQUID system as described by Weeks et al. (1993). Magnetic susceptibility (MS) and Anisotropy of MS (AMS) were determined on a KLY-2 induction bridge. Thermomagnetic curves were obtained by heating dried sam-

ples (0.1 to 0.4 g) in air to 700 °C in an automatic recording transversal Curie balance in magnetic fields ranging from 0.3 to 0.6 T.

The > 63 μm size fraction was isolated via wet sieving, and the < 63 μm size fraction was analyzed on a Micromeritics Sedigraph 5100.

Smear-slides for calcareous nannofossil counts were made at 5-cm intervals from raw sediment samples, following standard procedures (Haq and Lohmann, 1976). Fifty fields of view were examined between crossed nicols from each of the 161 smear-slides investigated. The smear-slides were investigated at 1250 × magnification, at a view-field diameter of 0.17 mm. The taxonomy follows Gard and Backman (1990). Foraminifers and ostracodes were examined in the > 150 μm size fraction.

### 4. Results

#### 4.1. Acoustic stratigraphy and coring sites

We present data from four cores collected from a North–South transect along the Lomonosov Ridge crest (Fig. 1) which were located close to chirp sonar profiles (Fig. 2, Table 1). The cores were selected from areas showing significant variations in acoustic stratigraphy as revealed by chirp sonar results.

Core 96/B8-1pc is 645 cm long and was raised from the slope towards the Makarov basin at a water depth of 1261 m, 13.2 km NNE from core PS2185-6 (Fütterer, 1992). The adjacent chirp sonar record (960902-49) is of relatively poor quality, but, nevertheless, the acoustic stratigraphy indicates sediments draping the ridge slope with no recognizable erosional features.

Core 96/13-1pc recovered 456 cm of sediments from the flat ridge crest at a water depth of 978 m. The chirp sonar record (960810-33) near this site shows abundant hyperbolic reflections, the result of the drape of the most recent sediments over an erosional surface which is indicated by an unconformity about 3 m below the sea-floor. The acoustically semi-transparent to transparent Unit 4, usually observed above the erosional surface, appears to be absent in this profile. However, this coring site is located approximately 260 m from the chirp sonar track and thus we cannot preclude the existence of the transparent unit at this site.

<sup>1</sup> <http://www.elsevier.com/locate/gloplacha>, see electronic appendices.

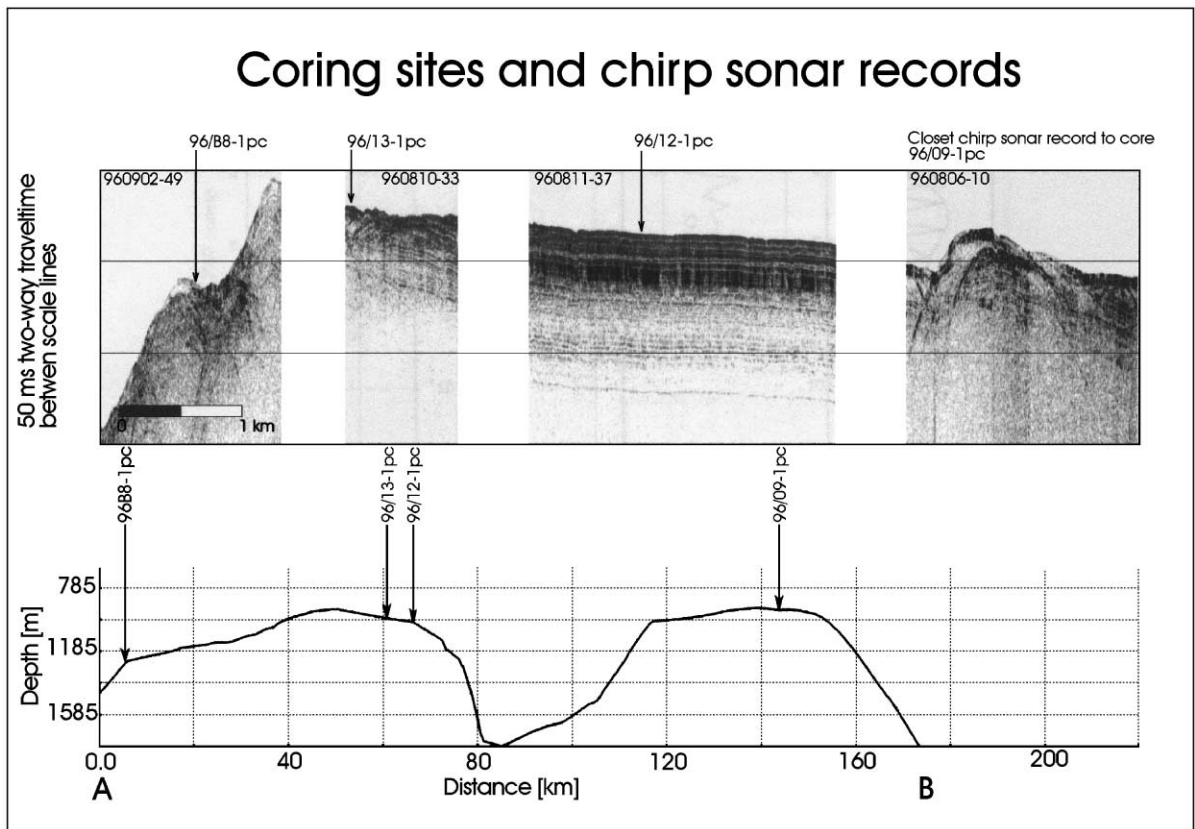


Fig. 2. Examples of chirp sonar profiles acquired from the Lomonosov Ridge crest during the *Arctic Ocean-96* expedition. The locations of the profiles are indicated in Fig. 1.

Core 96/12-1pc was raised from a water depth of 1003 m on chirp sonar profile 960811-37. High-quality sonar reflections reveal a smooth sea-bottom surface and an apparently undisturbed acoustic stratigraphy containing no obvious indications of erosion. This core has been selected as a reference for the core/seismic integration calculations, and was used for age model construction.

Core 96/09-1pc (270 cm) was raised from 927 m water depth and is located in Area 2 (Fig. 1). The nearby chirp sonar profile (960806-10) indicates unconformable sediments below an erosional surface.

#### 4.2. Lithology

Summaries of the major lithologies observed in the cores are presented in Fig. 3, and detailed stratigraphic descriptions for the individual cores are available in the electronic appendix.<sup>1</sup>

Cores 96/B8-1pc and 96/12-1pc display no obvious evidence of major sediment erosion, while cores 96/13-1pc and 96/09-1pc contain overconsolidated sediments (see physical properties section below) of unique lithology in the lowermost portions of the cores. All cores exhibit similar lithostratigraphy in the uppermost units which we briefly summarize here.

The uppermost unit is brown silty clay which ranges in thickness from 3 to 24 cm; the variation in unit thickness is partially due to incomplete recovery in the tops of piston cores. Below the dark brown clay, the sediment is composed of yellowish brown to yellowish gray silty clay, with some reddish sand layers (mm scale) in the lower part of the unit. This unit ranges from 60 to 111 cm thick. There is quartz and lithic fragment sand-size material in this unit, and it has a sharp contact with the underlying homogeneous dark gray silty clay (light olive gray in core

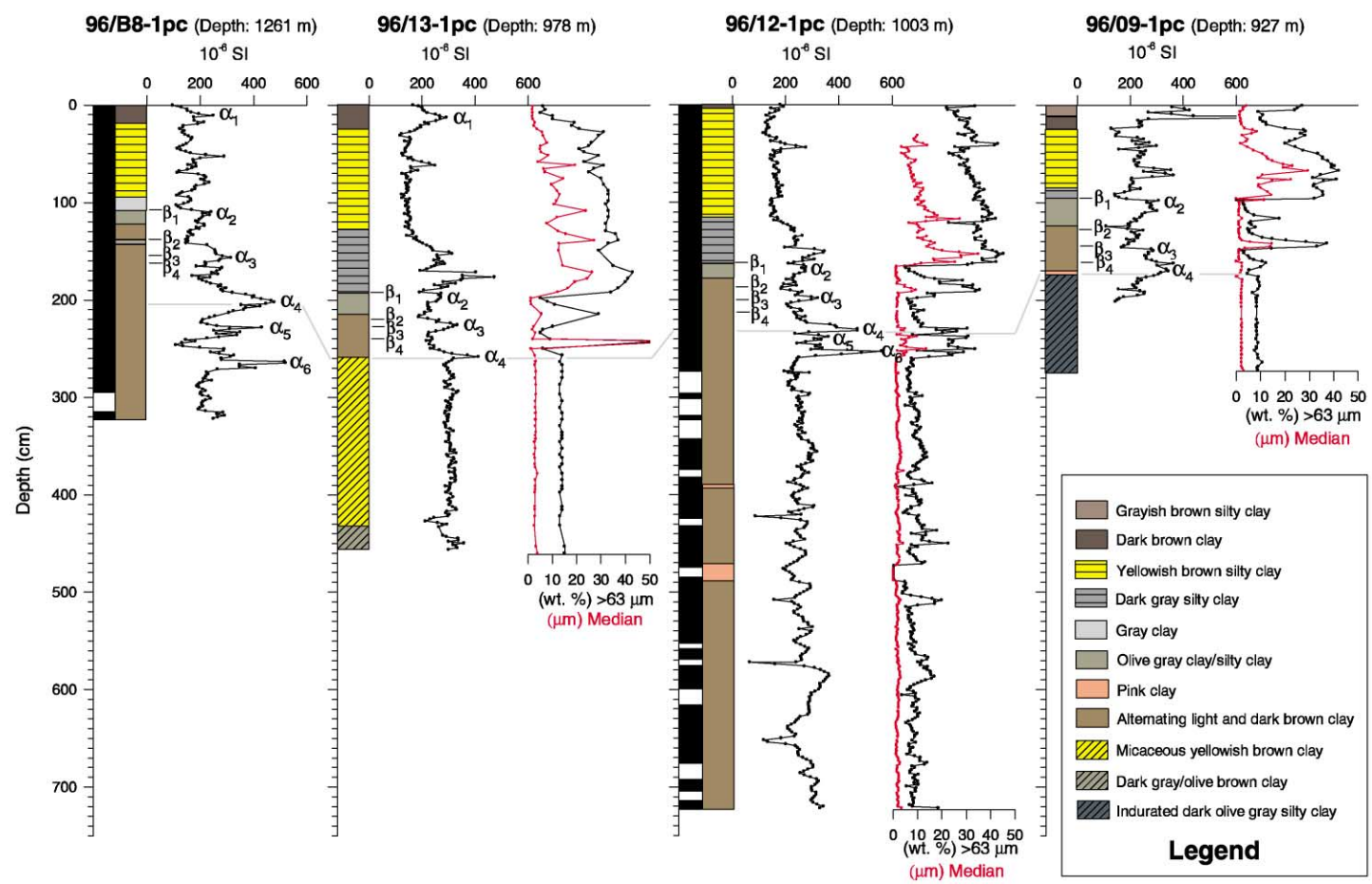


Fig. 3. The lithology, susceptibility, median grain size and > 63  $\mu\text{m}$  weight percent for the study cores collected along the bathymetric profiles A–B, indicated in Fig. 1. See Fig. 13 for the identification of paleomagnetic excursions.

96/B8-1pc) with thicknesses from 11 to 66 cm. A 1-cm-thick light gray clay unit with sharp upper and lower contacts is observed beneath the dark gray clay in all cores except core 96/B8-1pc. An olive to yellowish-gray silty clay with sharp upper and lower contacts occurs below the light gray clay, and it ranges from 13 to 36 cm in thickness. Below this, the cores are comprised of alternating dark and light brown clay units. These alternating units commonly display black speckles, mottles or banding in the dark brown units and occasionally in the lighter units. Contacts between the dark and light brown clay are usually gradational. These alternating dark and light brown sediments occur throughout the remainder of cores 96/12-1pc and 96/B8-1pc. A unique pink sediment is observed within a light brown sediment from 390 to 393 cm and 471 to 488 cm in core 96/12-1pc.

In core 96/09-1pc, these alternating units occur down to 171 cm. An extremely fine grained pink clay layer occurs at 171–173 cm. There is an abrupt change in the sedimentation at 173 cm which marks the top of a strongly indurated dark olive gray interlaminated (few mm) unit which extends down to 270 cm. This unit has a sharp bottom contact with an alternating light and dark gray clay unit at the bottom of the core (270–274 cm).

In core 12/13-1pc, the alternating light and dark brown units occur down to 259 cm. Below this, there is a 1-cm-thick light brown sand layer from 259 to 260 cm. Beneath the sand, there is an abrupt change in the sediment to a very micaceous yellow brown silty clay from 260 to 433 cm. At 433 to 437 cm, dark gray clay surrounds a 5-cm shale and calcite clast. A thin (437–440 cm) light olive brown clay with some reddish mottles grades into the final unit of olive brown silty clay through 456 cm.

#### 4.3. Sediment physical properties and grain size

Several pronounced density features (labeled  $\beta_1$  to  $\beta_4$  in Fig. 4) are present in the four GRAPE records from all cores. All cores reveal a near steady increase in bulk density with depth until between 94 cm (96/09-1pc) and 194 cm (96/13-1pc) (Fig. 4). Following this increase, an abrupt density decrease occurs in all cores, which coincides with the base of the dark gray sediment in cores 96/09-1pc, 96/12-

1pc, and 96/13-1pc, and the light olive gray sediment in core 96/B8-1pc. Stratigraphic correlation based on the prominent density features,  $\beta_1$  to  $\beta_4$ , results in a consistent lithologic correlation between the cores. A remarkably large change in bulk density is observed at 170 cm in core 96/09-1pc where the density increases from 1.71 to 2.00 g/cm<sup>3</sup> across a 10-cm interval, corresponding to the top of the indurated interlaminated unit. In core 96/12-1pc, a 17-cm interval with anomalously low density ( $\sim 1.43$  g/cm<sup>3</sup>), corresponds to the pink clay layer at 471–488 cm (Fig. 4).

The undrained shear strength ( $S_u$ ) generally increases with depth suggesting normal consolidation behavior in all cores except for in the lower parts of cores 96/13-1pc and 96/09-1pc (Fig. 5). Both these cores are retrieved from the areas of the Lomonosov Ridge where erosion is evident from the acoustic surveys and the lithologic changes described above. In core 96/13-1pc, a slight increase in shear strength can be seen from 340 cm and downwards. Shear strength in core 96/09-1pc increases rapidly at 170 cm, corresponding to the top of the indurated interlaminated unit to a maximum of 112 kPa at 260 cm. This value indicates over-consolidation of the sediments below 170 cm. The observed maximum shear strength of 112 kPa in core 96/09-1pc is equivalent to a sediment burden of approximately 37 m, calculated using a  $c/p$  ratio of 0.4 and a sediment bulk density of 1.8 g/cm<sup>3</sup>. An alternative consolidation test using an odometer was performed on a single sample from 216 to 218 cm, applying the one-dimensional method of Casagrande (1936). This test resulted in a pre-consolidation stress ( $P'_c$ ) of approximately 264 kPa which is equivalent to a depth of 35 mbsf for normally consolidated sediments (density 1.8 g/cm<sup>3</sup>), which is in excellent agreement with the  $c/p$  ratio result (37 m).

The grain size in cores 96/09-1pc, 96/12-1pc and 96/13-1pc (96/B8-1pc was not analyzed) shows considerable variability in the upper part of the cores (Fig. 3), and these variations are correlable above susceptibility feature  $\alpha_4$ . The oldest correlable grain size feature observed in all three cores is a short, high amplitude peak in both median grain size and  $> 63 \mu\text{m}$  content which occurs in a light (olive) brown unit centered at 215 cm in core 96/13-1pc, 190 cm in core 96/12-1pc, and 145 cm in core

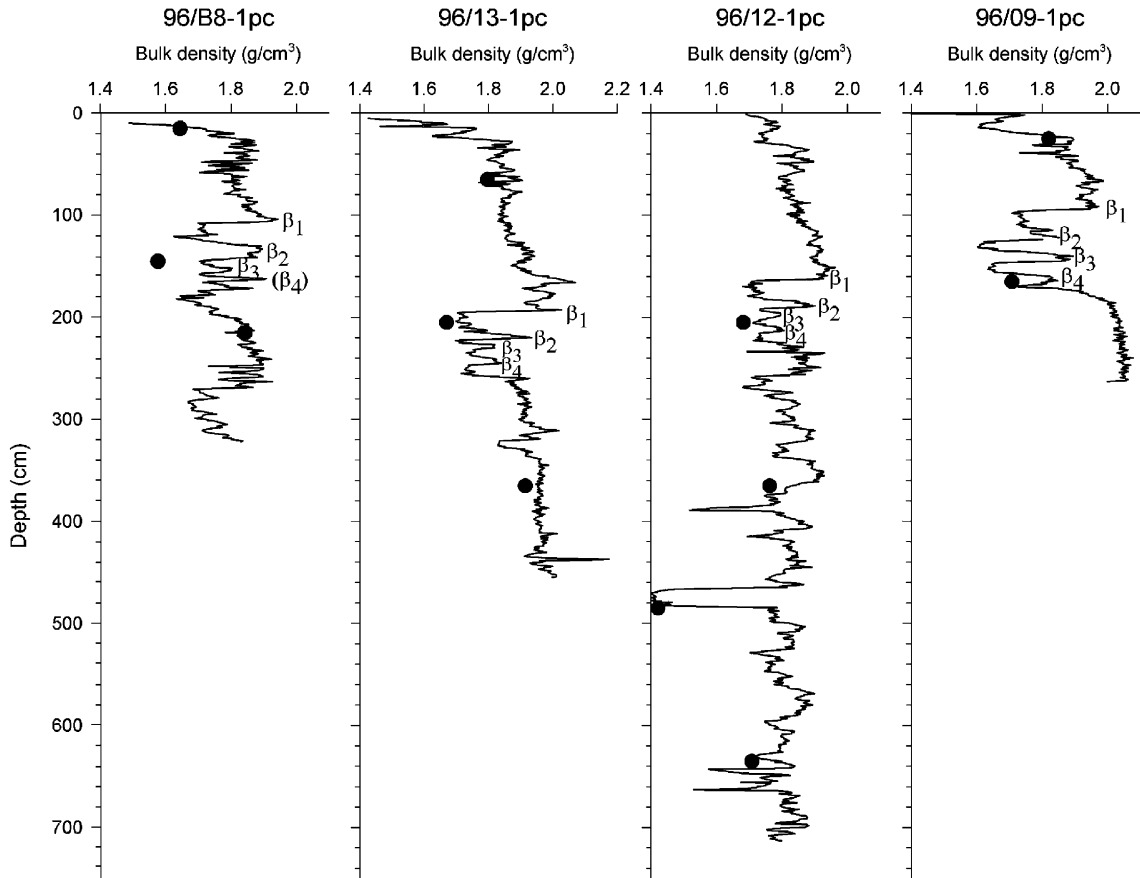


Fig. 4. GRAPE measurements derived from MST logging of the sediment cores. The GRAPE density is used as an estimate of sediment bulk density. Dots represent constant volume samples for which density was determined.  $\beta_1$ – $\beta_4$  represent pronounced density peaks used for correlation.

96/09-1pc. There is a dramatic increase (from  $\sim 2.5$  to  $15 \mu\text{m}$  for median size, and from 10 to 35 wt.% for  $> 63 \mu\text{m}$ ) in the grain size at the base of the dark gray units in all cores; grain size then decreases slightly toward the top of the gray unit. There is another increase in grain size at the base of the yellow silty clay unit, followed by a small, gradual, decrease and a final increase near the top of the yellow silty clay unit. The median grain size for the yellow silty clay is  $\sim 9 \mu\text{m}$ , with an average  $> 63 \mu\text{m}$  of  $\sim 30$  wt.%. The oxidized sediments at the top of the cores are marked by a final decrease in grain size. There is no appreciable difference in the grain size between cores in these correlable sediments.

The grain size is essentially constant below susceptibility feature  $\alpha_4$  (see mineral magnetic properties below) in cores 96/09-1pc (indurated layer, median =  $2.1 \mu\text{m}$ ) and 96/13-1pc (micaceous layer, median =  $3.0 \mu\text{m}$ ), but shows some high frequency, generally low amplitude variation in core 96/12-1pc in the alternating dark and light brown clays. The light brown sediments are slightly coarser (median =  $2.3 \mu\text{m}$ ) than the dark brown clays (median =  $1.8 \mu\text{m}$ ). The exception to this low amplitude signal is observed from 225 to 260 cm in core 96/12-1pc, where a sharp peak in the median grain size and percent of  $> 63 \mu\text{m}$  occurs; another slightly smaller peak occurs from 186 to 193 cm. The light pink clay units in core 96/12-1pc at 390–393 cm and 471–488

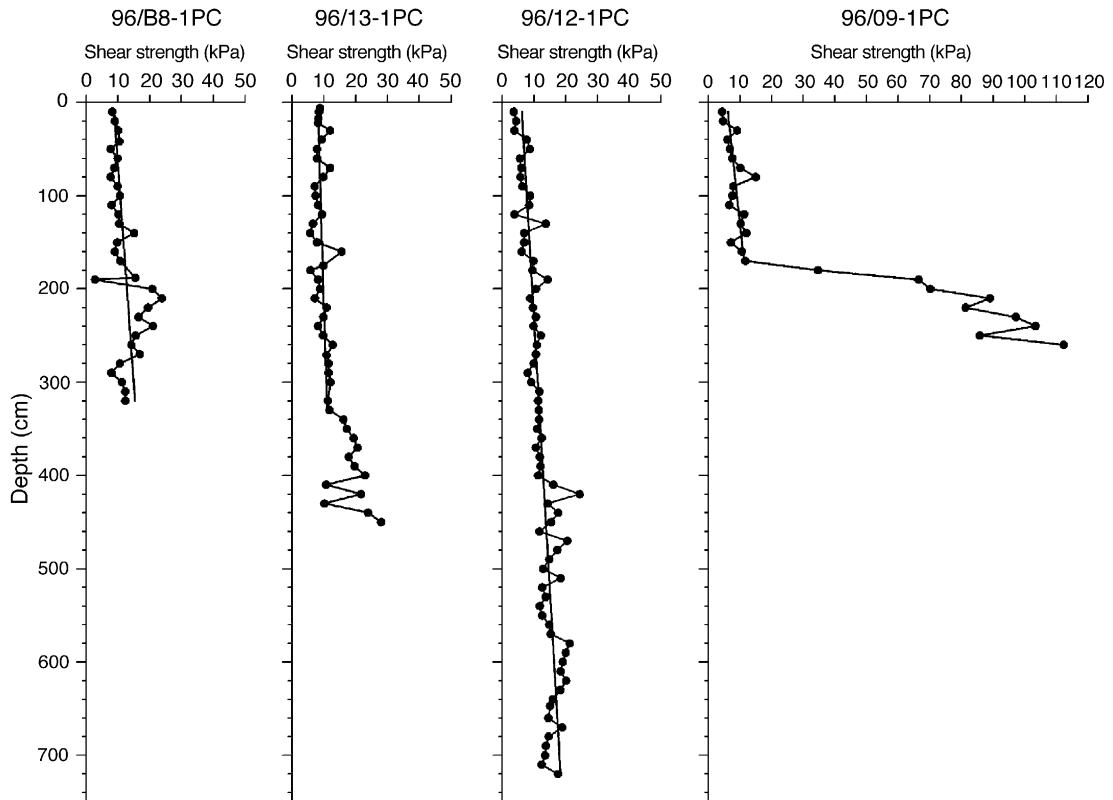


Fig. 5. Sediment shear strength measurements carried out on the sediment cores. The lines represent linear regressions of the shear strength values.

cm are comprised of essentially 100%  $< 2 \mu\text{m}$  material.

#### 4.4. Mineral magnetic properties

Susceptibilities range between  $1 \times 10^{-4}$  and  $10 \times 10^{-4}$  SI, with several pronounced features labeled  $\alpha_1$  to  $\alpha_6$  enabling stratigraphic correlation between the cores (Fig. 3). Feature  $\alpha_4$ , the lowest correlable susceptibility feature in all cores, always occurs in a light brown clay and is located just above the major sedimentary discontinuities in cores 96/09-1pc and 13. While there are specific susceptibility features, which can be used for core correlation, there is, in general, no systematic correspondence between variations of susceptibility and lithologic boundaries.

The  $S_{0.3}$ -factor, defined as the ratio  $\text{IRM}_{-0.3\text{T}}/\text{SIRM}$  is routinely used to monitor variations in

magnetic coercivity which often reflect lithological changes (Thompson and Oldfield, 1986). Low coercivity (soft) magnetic minerals such as members of the titanomagnetite series ( $\text{Fe}_{3-x}\text{Ti}_x\text{O}_4$ ,  $0 \leq x \leq 1$ ) and their low-temperature oxidation products are characterized by S-values close to  $-1$ , while hexagonal iron-oxide phases, such as hematite, typically have positive S-values. We have applied a modified S-factor defined by the ratio  $S_{0.1}/S_{0.3}$  believed to be a more sensitive indicator for variations of magnetically soft constituents.

The modified S-factor in general varies around 0.5 (Fig. 6). In cores 96/09-1pc, 12 and 13 distinct intervals with higher S-factors correspond to the dark gray, light gray, and olive gray sediment sequence, indicating completely different magnetic mineralogies in these intervals. An interval with S-values lower than 0.5 is observed in core 96/12-1pc in the alternating light and dark brown clay units below

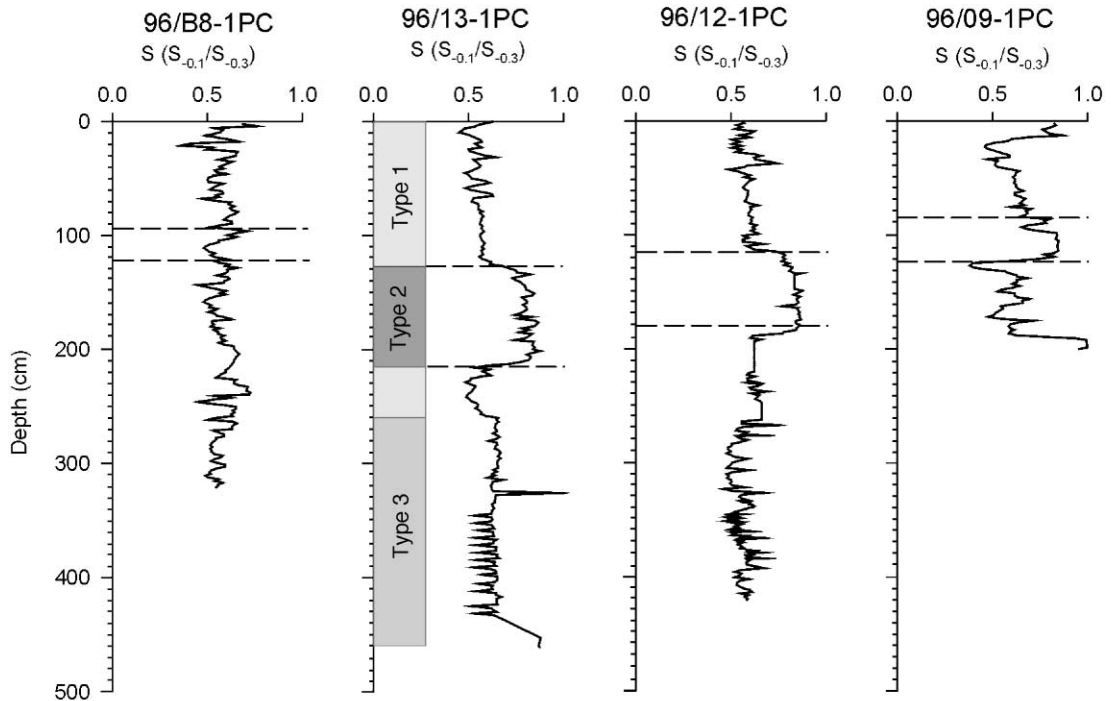


Fig. 6. S-ratio plotted with depth. The olive gray and dark gray silty clay units are shown with dotted lines for reference. Types 1, 2 and 3 refer to three distinct magnetic mineral assemblages derived from hysteresis properties. See electronic appendix for details.

260 cm, corresponding to the shift in grain size variability at this level.

Thermomagnetic analyses of 51 samples and magnetic hysteresis curve properties of 40 samples from core 96/13-1pc have been carried out and the results are available in the electronic appendix.<sup>1</sup> The hysteresis results generally show mineral magnetic properties that indicate the presence of magnetite-related minerals, in agreement with the results reported from the detailed investigation of PS2185-6 (Frederichs, 1995).

#### 4.5. Magnetic fabric

Anisotropy of magnetic susceptibility (AMS) was determined on all samples from the cores. Mineral magnetic constituents are dominated by titanomagnetite/maghemite assemblages justifying the interpretation of AMS in terms of depositional fabric (see electronic appendix). Magnetic fabric, derived from the lengths and directions of the principal susceptibility axes ( $k_{MAX}$ ,  $k_{INT}$ ,  $k_{MIN}$ ), is characterized by

foliation dominated ellipsoids (oblate) generally associated with sub-vertical minimum-axes ( $k_{MIN}$ ) and sub-horizontal maximum axes ( $k_{MAX}$ ) indicative of a primary depositional fabric (Tarling and Hrouda, 1993). Departures from this pattern occur in several more or less well-defined intervals in the upper ca. 2 m in all cores (Fig. 7). The stratigraphic consistency of these intervals between the cores indicates that these features are primary (pre-coring) features reflecting some regional process modifying the primary depositional fabric. The Holocene brown clay at the top of some cores and the sandy layers observed in the lower part of the yellowish brown clayey silt occur in the same intervals as these deviations in  $k_{MIN}$  and  $k_{MAX}$ .

Core A96/12-1pc exhibits shallow inclinations in  $k_{MIN}$  between 350 and 400 cm either reflecting natural conditions (Ellwood, 1984) or disturbances imposed during coring, transportation or storage of the cores. However, this interval with anomalously shallow  $k_{MIN}$  inclinations is also reflected by a distinct pattern in the anisotropy factor suggesting

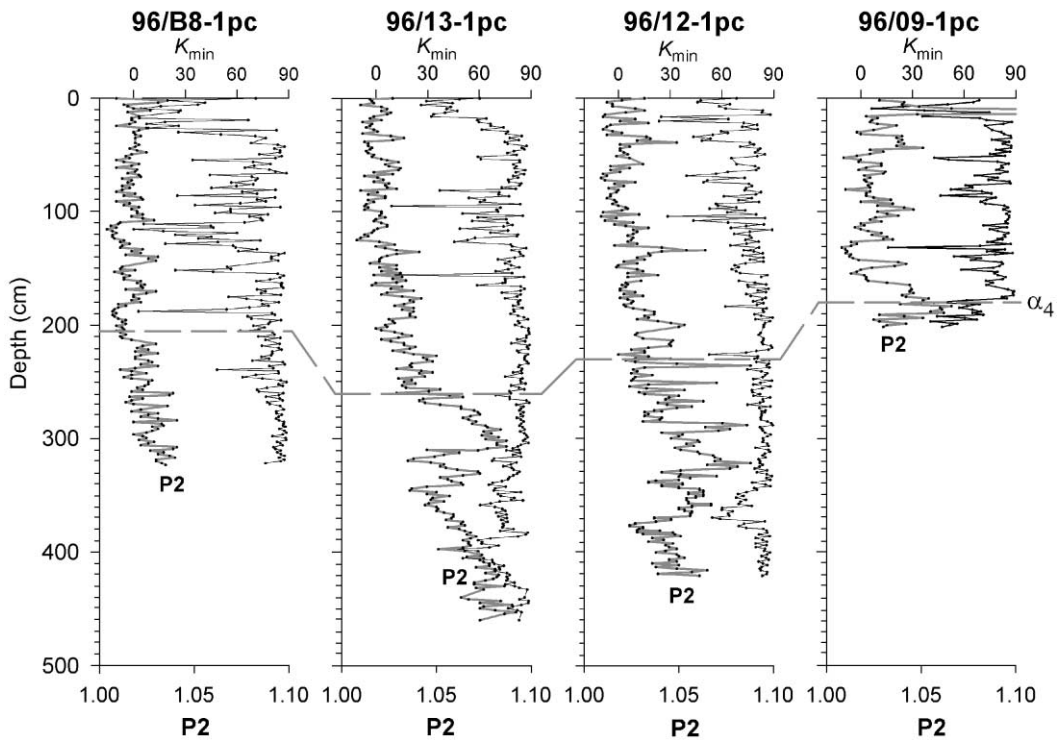


Fig. 7. Stratigraphic variations of anisotropy (P2) and inclinations of the  $k_{\text{MIN}}$  principal susceptibility axis of the susceptibility ellipsoid for the study cores.

the action of sedimentary processes. The anisotropy factor ( $P2 = k_{\text{MAX}}/k_{\text{MIN}}$ ) varies between 0.8% and 5%, which is in the range expected for a primary depositional fabric.

Core 96/09-1pc is characterized by several short zones with anomalously shallow  $k_{\text{MIN}}$  inclinations (Fig. 7). Abrupt changes in susceptibility have been related to depositional hiatuses, but discontinuities in susceptibility do not appear to be generally related to AMS properties, nor does susceptibility, in general, appear to be associated with major lithology changes. At 180 cm depth, there is a distinct change in both  $k_{\text{MIN}}$  and  $k_{\text{MAX}}$  inclinations and anisotropy (P2). This corresponds to the top of the indurated unit, which is associated with a 10 times increase in shear strength as well as discontinuities in the seismic records. The significant increase in  $k_{\text{MAX}}$  inclinations suggests either tilted beds ( $15^\circ$ ), deposition on inclined surfaces or some sort of shear deformation. We observed cross-laminated and truncated laminae

in the dark olive gray indurated sediment, likely the product of current activity.

#### 4.6. Nannofossil biostratigraphy of core 96/12-1pc and 96/12-1twc

The content of calcareous nannofossils was investigated at 5 cm sample intervals from the piston core and associated trigger weight core at site 96/12. Previous nannofossil work in the Eurasian part of the Arctic Ocean is summarized in Gard and Backman (1990). Baumann (1990) provided data from the Nansen Basin and Gakkel Ridge, and Gard (1993) provided data collected along two transects between the Eurasian shelf and the Lomonosov Ridge, including core PS2185-6, which was retrieved less than 50 km from core 96/12-1pc on the Lomonosov Ridge (Fig. 1).

Two taxonomic categories, *Gephyrocapsa* spp. and *Emiliania huxleyi*, are plotted in Fig. 8. Only the

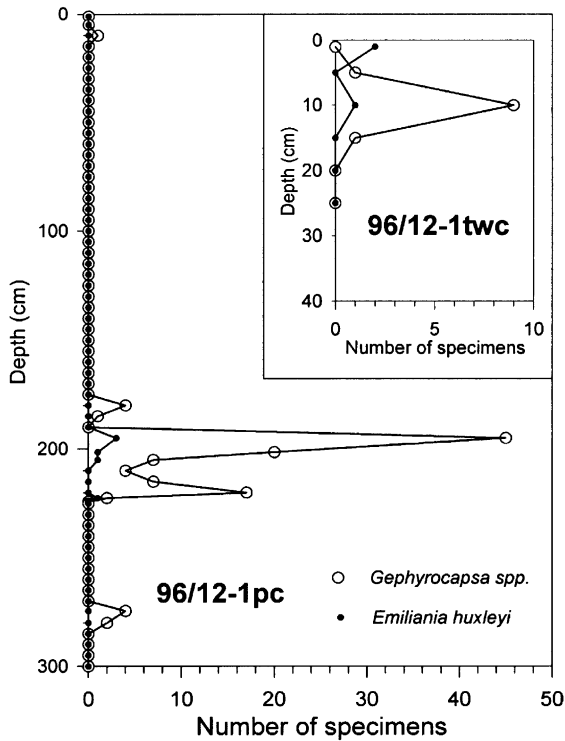


Fig. 8. Nannofossil census data from core 96/12-1pc and 96/12-1twc. Only the upper 300 cm of the 722 cm long core 96/12-1pc are shown because these taxa were not observed below 285 cm.

upper 300 cm of the 722 cm long core 96/12-1pc are shown because nannofossils were not observed below 285 cm. The 180–222.5-cm interval is dominated by *gephyrocapsids*, whereas the rare occurrences in two samples from 274.5 and 280 cm contain a mixture of *G. muelleriae* and the small species *G. aperta*. A specimen of *Coccolithus pelagicus* was observed at 201 cm. The *G. muelleriae* morphotype was observed at 258 cm.

The interpretation of the results from core 96/12-1pc relies on the fact that *E. huxleyi* evolved during oxygen isotope stage 8 (Thierstein et al., 1977) and on the idealized Nordic Seas sequence of Gard and Backman (1990, Fig. 8). The co-occurrence of *E. huxleyi* and *G. muelleriae* in the trigger weight core and their co-occurrence with *C. pelagicus* at 201 cm imply that (1) the nannofossils in the trigger weight core represents the Holocene (oxygen isotope stage 1) and (2), the abundance peak centered on 195 cm represents oxygen isotope stage 5.1 and the peak

centered on 220.5 cm represents stage 5.5. It is not known if the small peak centered on 180 cm represents reworking or indigenous occurrences. The small peak centered on 274.5 cm probably represents an indigenous occurrence, as there is no source material available down-core for reworking. Based on the species composition, these two samples belong to the Pleistocene. The age model of Jakobsson et al. (2000) indicates that the nannofossils at 274.5–280 originated during interglacial stage 7.5.

Gard (1993) observed “traces of Quaternary nannofossils” at 186, 233 and 309 cm in core PS2185-6, correlated to depths of approximately 200, 222 and 260 cm in core 96/12-1pc. Finally, reworking of rare Cretaceous species such as *Watznaueria barnesae* occurs sporadically throughout the core.

#### 4.7. Foraminiferal stratigraphy of core 96/12-1pc and 96/12-1twc

Calcareous foraminifers (benthic and planktonic) and ostracodes occur almost exclusively in four intervals: 0–30 cm (twc), 165–185, 194–230 (three spikes), and 257–286 (two spikes) (Fig. 9). One sample outside these intervals, at 134 cm (core break), yields some planktonic foraminifers. Arenaceous benthic foraminifers occur in 206–227 cm and below 251 cm, to the base of the core. Generally, the foraminiferal species composition is common for the Arctic Ocean (e.g., Lagoe, 1977). Plankton is represented by *Neogloboquadrina pachyderma*, with overwhelmingly prevalent left-coiling forms. Benthic calcareous foraminifers are dominated by high percentages of *Cassidulina teretis* (up to 92%), the most abundant species at water depths between 600 and 1200 m throughout the Arctic Ocean (e.g., Polyak, 1990).

The presence of only arenaceous foraminifers below 287 cm in 96/12-1pc likely indicates carbonate dissolution due to corrosive waters and/or lower sedimentation rates (cf. O’Neill, 1981; Ishman et al., 1996). The spiky distribution of both calcareous and arenaceous forms within the upper 287 cm presumably reflects abrupt productivity changes in the Arctic Ocean. This interpretation is consistent with the occurrence of faunal spikes only in dark brown units corresponding to interglacial periods. Superimposed

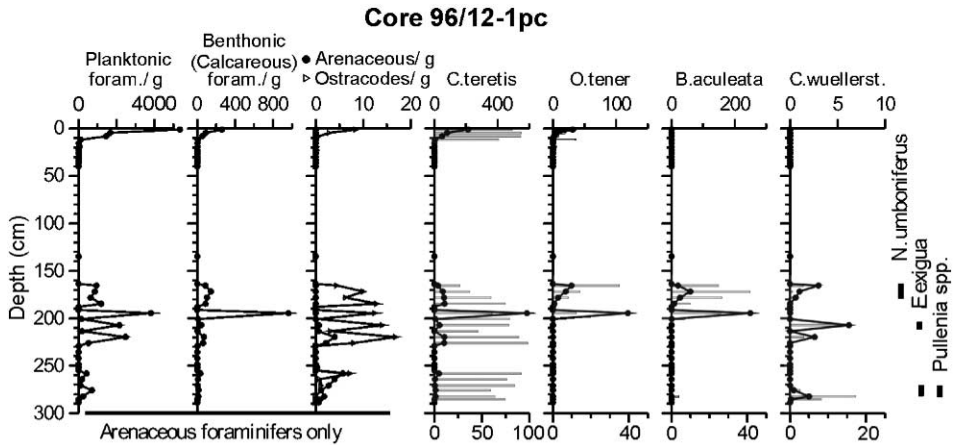


Fig. 9. Down core distribution of foraminifers and ostracodes in 96/12-1 (size fraction  $> 150 \mu\text{m}$ ). Lines show absolute numbers per gram of dry sediment (scale on top), bars show percentages of major benthic calcareous foraminifers (scale at the bottom). Note that scales vary between species. Vertical bars on the right show the occurrence range of selected accessory species.

on foraminiferal abundance spikes, the down-core distribution of benthic foraminiferal species shows a distinct stratigraphic zonation (Fig. 9). The most

apparent changes in species composition include: (1) the presence of *Cibicidoides wuellerstorfi* at several intervals below 165 cm, with maximum percentages

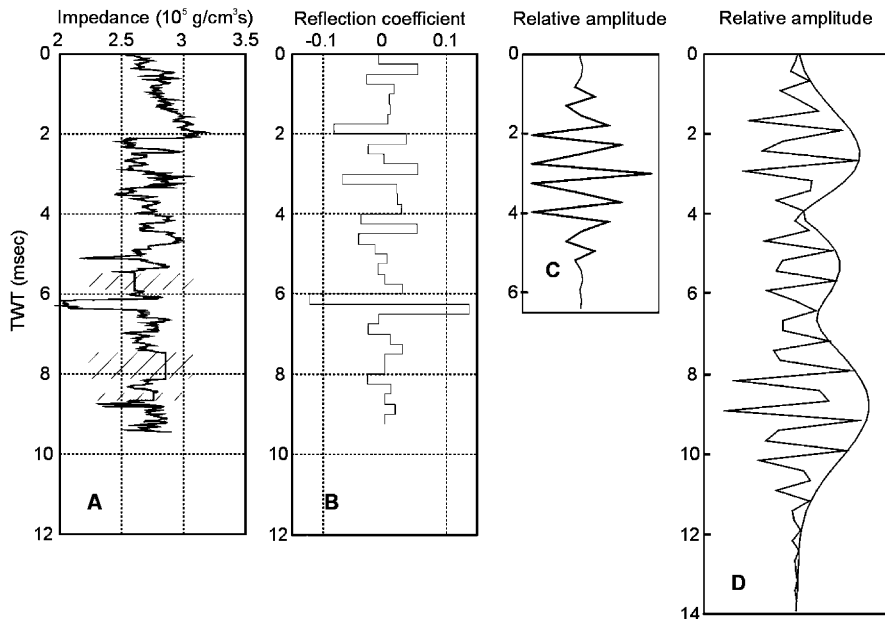


Fig. 10. (A) Calculated impedance log versus two-way travel time in milliseconds for core 96/12-1pc. The hatched areas indicate intervals in the core where constant values were assigned, by assigning the value directly above the interval in the p-wave log, as well as in the GRAPE log, before calculating the impedance log. (B) The reflectivity function for core 96/12-1pc sub-sampled at 8 kHz. (C) The wavelet corresponding to the chirp sonar pulse, 2–4 kHz, calculated by the minimum four-term Blackman–Harris window as described by Schock et al. (1989). (D) Synthetic seismogram for core 96/12-1pc resulting from convolution between the wavelet corresponding to chirp pulse 2–4 kHz in (C) and the reflectivity function in (B).

at 207 and 282 cm, (2) a consistent occurrence of *Oridorsalis tener* above 195 cm, reaching 35% at 165 cm, and (3) occurrence of *Bulimina aculeata* at 165 and 200 cm (up to 41% at 172 cm) and in one sample at 282 cm. Some accessory species, not common for the modern Arctic Ocean, occur in 96/12-1pc at some levels: *Nuttalides umboniferus* at 165–178 cm, *Epistominella exigua* at 220 and 275–282 cm, and *Pullenia* spp. at the latter interval.

#### 4.8. Core/seismic integration (synthetic seismograms)

Acoustic stratigraphy based on chirp sonar results revealed compelling evidence of erosional activity over the Lomonosov Ridge crest rise (Jakobsson, 1999). The termination of the erosional phase is indicated by reflector A at approximately 4 ms (TWT) sub-bottom, which is within the range of piston coring. A synthetic seismogram has been computed for core 96/12-1pc in order to determine the relationships between acoustic reflector A (identified in profile 960811-37 crossing this coring site, Figs. 1 and 2) and the physical properties of the sediments

(Fig. 10A). For a description of the synthetic modeling procedure see the electronic appendix.<sup>1</sup>

In some parts of core 96/12-1pc, the p-wave velocity measurements did not yield reliable values. In order to minimize the effect of these intervals on the calculated impulse response and thus on the synthetic seismogram, constant values were assigned by using the p-wave log value directly above the interval. The calculated impedance log is shown versus two-way travel time in Fig. 10A. The reflectivity function was calculated using this impedance log, and is shown sub-sampled at 8 kHz in Fig. 10B. A simulated reflection for the water/sediment interface was achieved by assigning a bottom water velocity of 1450 m/s and a density of 1.028 g/cm<sup>3</sup> (CTD measurements carried out from *Oden*; P-I Sehlstedt, pers. comm.). The computed synthetic seismogram resulting from convolution between the compressed wavelet corresponding to the chirp pulse 2–4 kHz (Fig. 10C) and the reflectivity function for core 96/12-1pc reveals three large reflectors at 2.5, 5.3 and 8.7 ms (Fig. 10D). The first reflector (2.5 ms) is due to the impedance contrast from the simulated water/sediment interface. The second reflector

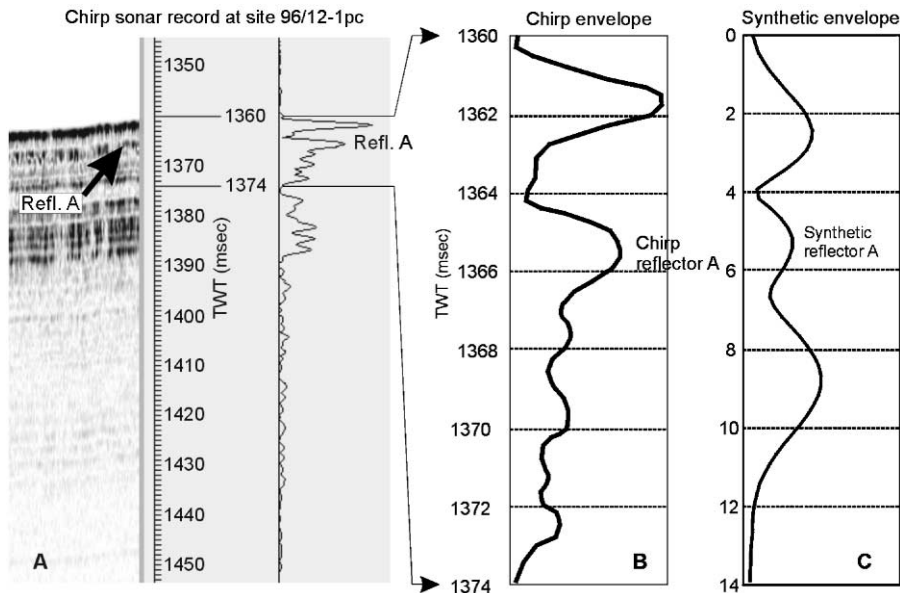


Fig. 11. (A) Chirp sonar record at site 96/12. (B) Chirp envelope between 1360 and 1374 ms (TWT). (C) Synthetic envelope for core 96/12-1pc. A correlation is suggested between the uppermost chirp sonar acoustic reflector A and the first synthetic reflector below the simulated sediment/water interface (synthetic reflector A).

(5.3 ms), is located 2.8 ms below the water/sediment interface (5.3–2.5 ms) and may arise from constructive interference composites caused by several smaller impedance contrasts associated with the top of the olive gray clay and the upper part of the dark/light brown sediments in a manner such as demonstrated by Mayer (1979). The peak relative amplitude of the third reflector occurs at a depth of 6.2 ms below the water/sediment interface (8.7–2.5 ms), the deepest significant reflector in the computed synthetic seismogram for core 96/12-1pc, which is likely associated with the large density decrease associated with the pink sediment layer at this depth.

The uppermost prominent acoustic reflector A, occurring at approximately 4 ms sub-bottom depth in chirp sonar profile 960811-37 at site 96/12-1pc, correlates with the first synthetic reflector at 2.8 ms below the simulated reflection for the water/sediment interface in core 96/12-1pc (Fig. 11). The discrepancy between the sub-bottom depths between the synthetic reflector and reflector A may be due to loss of the uppermost 30 cm of sediments in core 96/12-1pc during core retrieval and sediment compression during coring.

## 5. Discussion and conclusions

The cores from the Lomonosov Ridge fall into two categories: (1) Cores collected below 1000 mbsl from regions which show conformable and continuous seismoacoustic stratigraphy as well as undisturbed continuous sediments in the recovered core material. (2) Cores collected from above 1000 mbsl from areas which show unconformities in the seismoacoustic stratigraphy, which can be related to abrupt changes in sediment lithology and physical properties in the sediment cores.

The investigated area of the Lomonosov Ridge is located far away from the continents, and the cores were collected from relatively shallow depths. Therefore, the dominant terrigenous sediment input ought to be from ice rafting (sea ice or icebergs). In this environment turbidity currents are not an active transport mechanism, and we observe no signs of mass wasting on the shallow ridge crest in the chirp sonar records (Jakobsson, 1999). Therefore, removal

or non-deposition of the sediments is most likely from currents or ice grounding.

We observe generally continuous glacial–interglacial sedimentation in cores 96/12-1pc and 96/B8-1pc. This glacial–interglacial sedimentation is manifested as alternating dark and light brown clay units, which are continuous below about 1 m in core 96/B8-1pc and 1.8 m in core 96/12-1pc. The dark brown clays are characterized by high concentrations of manganese and common bioturbation, both indicative of well-oxygenated water, and fine particle size, indicative of reduced glacial input. The light brown clays are characterized by lower manganese concentration with little or no bioturbation, indicative of low oxygen concentration and coarser particle size, representing enhanced glacial ice sediment transport (Fig. 12). Below 260 cm (core 96/12-1pc), we interpret these light dark alternations as “distal” glacial–interglacial sedimentation, meaning that the site received some ice rafted material, but the amount of  $> 63 \mu\text{m}$  material is only approximately 10 wt.%, and the differences between glacial and interglacial coarse material are small. Above 260 cm, the contrast in grain size between glacial and interglacial sediments is significantly enhanced. This change occurs soon after a transition from arenaceous to mostly calcareous foraminiferal fauna at 287 cm. Additionally, indigenous nannofossils are observed in all the dark brown units above this depth (Fig. 12).

The sediment color and manganese variations were used to construct an age model via correlation with a low latitude oxygen isotope record (Jakobsson et al., 2000); this age model is internally consistent with both the nannofossil biostratigraphy (Fig. 8) and paleomagnetic excursions determined from core 96/12-1pc (Fig. 13). Oxygen isotope stages 1 through 21 are all inferred in core 96/12-1pc (Fig. 13).

The age model of Jakobsson et al. (2000) is inconsistent with several previously published age models derived for sediments from the central Arctic Ocean, and we recognize that our stratigraphy can be precisely correlated to cores with alternative age models. If we interpret the excursion we identified as Biwa 2 in core 96/12-1pc as the Bruhnes/Matuyama boundary, our stratigraphy, susceptibility, and grain size records are easily correlated with Frederichs' (1995), and Spielhagen' et al. (1997) results from Lomonosov Ridge cores PS2185-6 and PS2185-3

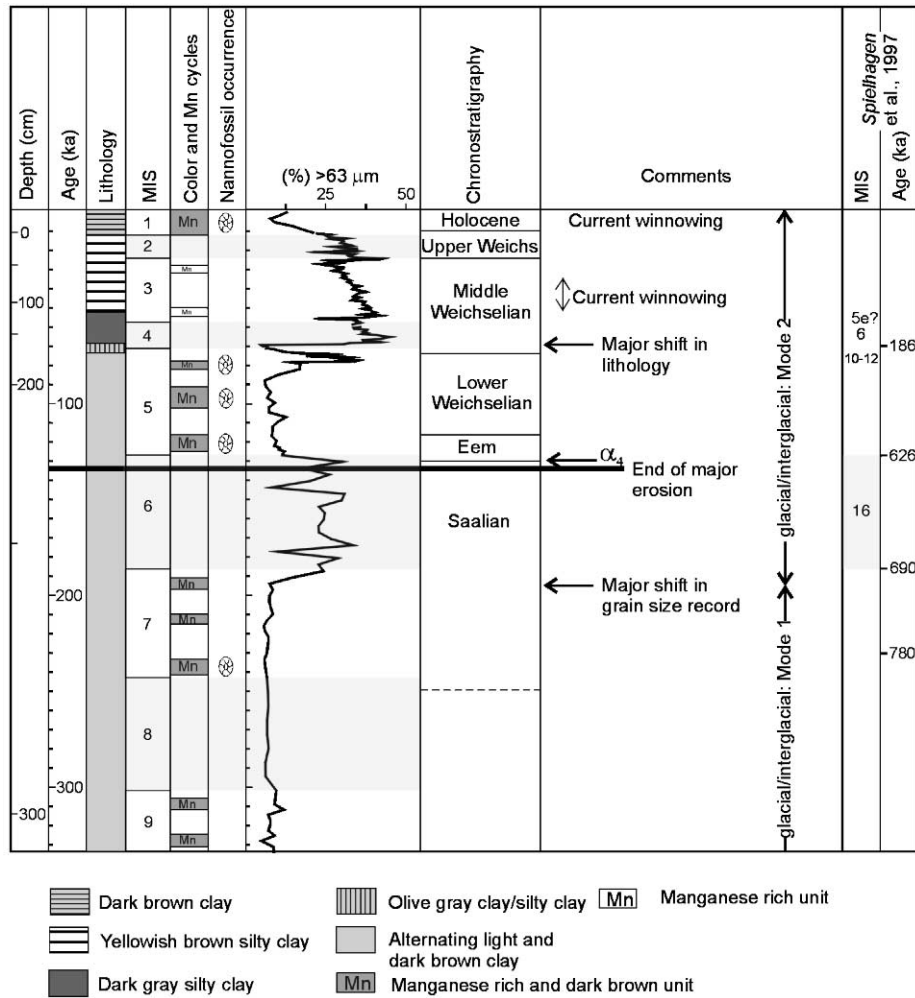


Fig. 12. Summary of major environmental changes for sediments from the Lomonosov Ridge based on core 96/12-1pc and 96/12-1twc. Land-based chronostratigraphic boundaries as defined by Larsen et al. (1999). In the intervals where unambiguous correlation to core PS2185-6 could be established (Fig. 13), the chronology suggested by Spielhagen et al. (1997) is shown.

(Fig. 13). In addition, the patterns of microfaunal distribution allow correlation between 96/12-1pc and core PS2185-6. The levels of planktonic foraminiferal spikes are almost identical in both cores; the only significant difference is an additional spike at ca. 20–30 cm in PS2185-6 (Spielhagen et al., 1997). The close correlation between the two cores is further supported by means of arenaceous foraminifers (Evans and Kaminski, 1998) and ostracodes (Jones et al., 1999). Moreover, the patterns of foraminiferal distribution provide a preliminary correlation of

96/12-1pc with distant Arctic Ocean sites such as the Mendeleev, Northwind, and Alpha ridges (O'Neill, 1981; Polyak, 1986; Scott et al., 1989; Poore et al., 1994; Ishman et al., 1996). A distinct microfaunal stratigraphic marker for this correlation is the boundary between almost entirely arenaceous to mostly calcareous assemblages that occurs in 96/12-1pc at 287 cm. The validity of this stratigraphic marker is confirmed by a benthic foraminiferal zonation, which is especially similar between 96/12-1pc and cores raised from similar water depths

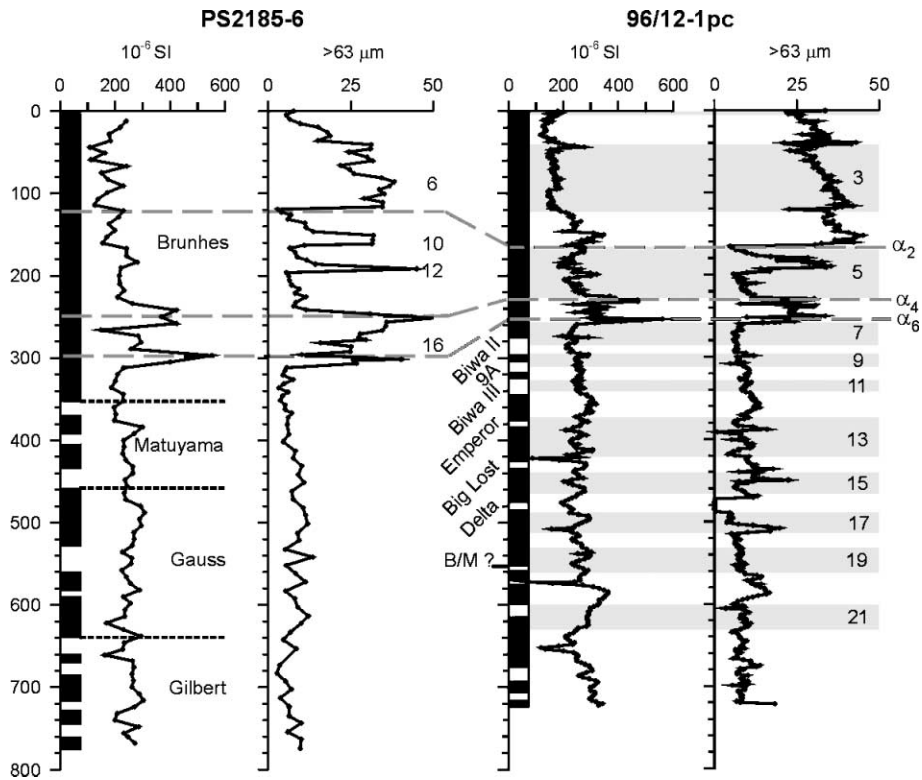


Fig. 13. Correlation between core PS2185-6 (Spielhagen et al., 1997) and 96/12-1pc.

at the Mendeleev and Northwind ridges (Polyak, 1986; Poore et al., 1994; Ishman et al., 1996).

In contrast to the uniform glacial/interglacial sedimentation described above, cores 96/09-1pc and 96/13-1pc show clear evidence for sediment erosion; the bottom portions of the cores contain dark olive-gray indurated sediments and micaceous yellow brown silty clay, respectively. The age of these sediments is unknown. Consolidation studies indicate either that approximately 33 m of sediment was stripped from above the indurated unit in core 96/09-1pc, or that the sediments were compacted by an external load. The median grain size is quite constant ( $2.1 \pm 0.5$ ) in this unit, and it displays mm scale color variations which are convoluted, and in some cases truncated by other colored intervals. There is no evidence of glacial/interglacial cyclical variability.

The lower part of the micaceous unit in core 96/13-1pc is slightly overconsolidated, but detailed

consolidation tests were not run. The unit is basically structureless, but black banding is observed in some intervals. The median grain size is constant ( $3.0 \pm 0.3$   $\mu\text{m}$ ), and there is no evidence of cyclical variability. The coarse grain size and a 1-cm-diameter dropstone at 373 cm suggest that this unit received iceberg-rafted detritus and was formed during glacial conditions. The concentration of clay size material in this unit is low compared with both the indurated unit in core 96/09-1pc, and the alternating dark and light brown layers in cores 96/12-1pc and 96/B8-1pc, suggesting that the micaceous sediment is associated with current winnowing. Additional support for winnowing is taken from the AMS studies, which indicate an increase in the anisotropy factor P2, and a decrease in  $k_{\text{MIN}}$  in the lower part of this unit (Fig. 7). The lack of cyclical variation could indicate deposition sometime prior to MIS stage 21, as this unit is not observed in cores 96/B8-1pc and 96/12-1pc. However, the micaceous sediment corresponds

to the transparent seismoacoustic Unit 4 observed in most of the eroded regions. Thus, an alternative explanation is that this unit might represent reworked sediment related to the large-scale erosional activities at the top of the Lomonosov Ridge crest.

The lithology, physical properties, grain size (Fig. 3), and the seismoacoustic stratigraphy (Fig. 2), illustrate that the sediments above the indurated and micaceous units are conformable and correlable with the continuous sedimentary records in cores 96/B8-1pc and 96/12-1pc. The core/seismic integration shows that reflector A, representing the base of seismoacoustic Unit 5, results from impedance contrasts from density features  $\beta_1$ – $\beta_4$ . The sediments which contain susceptibility feature  $\alpha_4$  are light brown clay in all cores and formed during the later part of MIS 6. Thus, the major erosional event ended in stage 6, although we cannot rule out current winnowing or short (less than one MIS) breaks in sedimentation in any core. In addition to the ability to correlate lithologies, the grain size variability changes character above this interval. The first “large amplitude” grain size peak occurs in core 96/12-1pc during MIS 6; this peak is missing in cores 96/09-1pc and 96/13-1pc due to the erosion. The next “large amplitude” peak occurs during stage 5.1, and is observed in all cores. The glacial stages 4 and 2 are also observed as large grain size increases in all cores. This suggests that the severity of glaciation increased and/or the transport of ice over these sites was more common starting in stage 6 and the site transited from a “distal glacial” sedimentary regime, to a “proximal glacial” sedimentary regime. Spielhagen et al. (1997) found smectite-rich sediments associated with increased amounts of coarse material in core PS2185-6, which is easily correlated with core 96/12-1pc. The main source for smectites in the central Arctic Ocean are the shelves of the Kara and western Laptev seas (Washner et al., 1999; Stein et al., 1994a), and Spielhagen et al. (1997) interpreted this coarse layer as an indication of substantial iceberg activity from northern Siberia. Thus, this major shift in amplitude of glacial/interglacial activity in the central Arctic Ocean was likely associated with enhanced glacial activity in northern Siberia. The lithologies of the sediment column above this glacial/interglacial amplitude shift display increased variability as well.

All cores contain alternating dark and light brown units from at least  $\alpha_4$  to the base of an olive gray silty clay, representing glacial and interglacial sedimentation, respectively. The olive gray unit, formed in the latest part of stage 5, is observed in all cores, but the color of this unit in core 96/B8-1pc is quite light and less distinct, although the density decrease associated with this unit is clearly visible (Fig. 4). In addition to the anomalously low density found in this unit, the grain size is slightly higher than the light–dark brown clays (median  $\sim 10 \mu\text{m}$ ) and it is associated with susceptibility feature  $\alpha_2$ . In all cores except core 96/B8-1pc, there is a distinctive 1-cm-thick light gray clay that forms the sharp upper contact of the olive layer. Above this, a dark gray sedimentary unit, formed during stage 4 and early stage 3, is characterized by coarse grain size (median grain size =  $15 \mu\text{m}$ ), anomalous magnetic mineral assemblages and sharp upper and lower contacts. Again, in core 96/B8-1pc, the unit is not well pronounced and only occurs as a light olive gray layer which does not display much variability in magnetic mineralogy. Core 96/B8-1pc was collected on the Amerasian side of the Lomonosov Ridge, and other investigators have noted the absence of the dark gray silty clay on the Amerasian side of the ridge as well as in sediments from the Makorov basin (Morris et al., 1985). Although we are able to identify a correlable sedimentary interval, the areally restricted distribution of this unit indicates that the Lomonosov Ridge acts as a barrier to some sedimentary source area or transport system. The yellow brown silty clay, formed during stages 2 and 3, is found in all cores and shows evidence of current winnowing from sandy layers in the bottom portion (stage 3) of the unit, has relatively coarse (median  $\approx 9 \mu\text{m}$ ) grain size (although this is also a function of the increased ice rafting to the site as indicated by the increase in grain size during stage 2) and the AMS parameters indicate current related sedimentation.

Magnetic fabric based on AMS has been used to infer the strength and direction of bottom-currents in deep-sea regimes (Ellwood and Ledbetter, 1979; Auffret et al., 1981). The core sections studied here have unknown azimuthal orientation and, hence, no direct information about current azimuths acting during deposition can be retrieved. However, variation

in  $k_{\text{MAX}}$  inclination is likely to be related to variations in current regimes. We have only presented inclinations of the  $k_{\text{MIN}}$  axis, but since both axes are orthogonal, the latter varies in accord with  $k_{\text{MAX}}$ . The anomalously shallow  $k_{\text{MIN}}$  ( $< 60^\circ$ ) directions occurring within several corresponding stratigraphic intervals in the cores cannot be attributed to normal water flow conditions (Fig. 7), and are generally associated with interglacial sediments in the cores. Anomalous  $k_{\text{MIN}}$  directions are associated with lower anisotropy factors (P2), which indicate the degree of statistical alignment of grains. The apparent relationship between the amplitude of inclination variation and degree of grain alignment indicates that other processes have dominated over gravity. Hence, we propose that the process may be current activity during interglacial periods.

The areas of the Lomonosov Ridge crest where we had observed evidence for substantial erosion during the *Arctic Ocean-96* expedition (Jakobsson, 1999) were subjected to a detailed survey using a Sidescan Swath Bathymetric Sonar during the submarine SCICEX expedition in 1999. The analyses of this data unambiguously indicate that this section of the ridge crest has been molded and scoured by a grounded ice sheet down to a modern water depth of 1 km (Polyak et al., 2001).

The extent and thickness of Pleistocene Arctic glacial ice is still the subject of much debate (e.g., Karlén et al., 1998; Thiede and Bauch, 1999). A single dynamic ice system consisting of terrestrial and marine grounded ice sheets and floating ice shelves has been discussed by several authors (e.g., Hughes et al., 1977; Grosswald, 1980; Denton and Hughes, 1981). A common, essential element in these hypotheses is the presence of a thick ice shelf in the central Arctic Ocean.

Observations suggesting ice grounding at substantial water depths include results from ODP Site 910 at the Yermak Plateau at 556 mbsl (Myhre et al., 1995); this glacial event is thought to have occurred prior to 660 ka (Flower, 1997). Relict plowmarks carved by the keels of huge icebergs are reported down to ca. 850 mbsl on the Yermak Plateau (Vogt et al., 1994), whereas, late Weichselian ice grounding at 630 mbsl has been reported from the St. Anna Trough on the Kara Sea margin (Polyak et al., 1997). Our core studies indicate that the ice grounding at

the Lomonosov Ridge crest took place during the later part of MIS 6, but according to an alternative age model (Spielhagen et al., 1997), this event occurred much earlier, at MIS 16.

In summary, sediment cores and seismoacoustic data show that sedimentation comprised continuous cyclic variations between glacial and interglacial conditions. Well-oxygenated water, some current activity and some ice rafting prevailed during interglacials. Less well-oxygenated water, ice rafting of coarse sediments and reduced (or non-detectable) current activity characterized glacials. The amplitude of the glacial–interglacial variability ramped up by the beginning of MIS 6 (Jakobsson et al., 2000 age model), indicating a major reorganization in glacial activity and corresponding paleoceanographic conditions in the Arctic Ocean, and sediments in the shallowest parts of the ridge were removed during a strong erosional event during this glacial stage. In combination with SCICEX-99 findings (Polyak et al., 2001), our data indicate that this erosion was caused by ice grounding at 1 km present water depth. It appears that the increased glacial activity was associated with ice sheets formed in northern Eurasia.

### Acknowledgements

The *Arctic Ocean-96* expedition was organized and executed by the Swedish Polar Secretariat. The generous support of the crew of the icebreaker *Oden* during numerous chilly moments on the aft deck is much appreciated. The help provided by Yngve Kristoffersen and Arne Lif during coring and chirp sonar operations is gratefully acknowledged. Jim Broda provided valuable advice during the construction of the piston corer. Jan Kristiansson provided the odometer test data. We are grateful to C. Kissel for assisting in the U-channel analysis and hysteresis measurements in the paleomagnetic laboratory, Gif-sur-Yvette. MST data were collected at AGC/BIO, Canada, and we acknowledge the help provided by Kate Moran, Matthew and Andrew Barret. Discussions with Larry Mayer on chirp sonar theory are appreciated. Marianne Ahlbom, Heather Renyck and Kristin Karsh performed the grain size analyses. This project was financed by the Swedish Natural Science Research Council, Stockholm University and the

Norwegian Research Council (mineral magnetic parameters). The contribution by Leonid Polyak was supported by NSF grant OPP-9817054. Reviews by Ruediger Stein and Peter Vogt significantly improved the manuscript.

## References

- Auffret, G.A., Sichler, B., Coléno, B., 1981. Deep-sea sediments texture and magnetic fabric, indicators of bottom currents regime. *Oceanol. Acta* 4, 475–488.
- Baumann, M., 1990. Cocoliths in sediments of the eastern Arctic Basin. In: Bleil, U., Thiede, J. (Eds.), *Geological History of the Polar Oceans: Arctic versus Antarctic*. NATO ASI Ser. C, vol. 308, pp. 437–445.
- Blasco, S.M., Borhold, B.D., Lewis, C.F.M., 1979. Preliminary results of surficial geology and geomorphology studies of the Lomonosov Ridge, Central Arctic Basin. *Curr. Res.-Geol. Surv. Can., Part C, Paper 79-1C*, pp. 73–83.
- Carmack, E., 1990. Large-scale physical oceanography of polar oceans. In: Smith, W.O. (Ed.), *Polar Oceanography, Part A, Physical Science*. Academic Press, San Diego, pp. 171–222.
- Casagrande, A., 1936. Determination of preconsolidation load and its practical significance. *Proceedings 1st Conference Soil Mechanics and Found. Am. Soc. Civ. Eng.*, vol. 3, pp. 60–64.
- Clark, D.L., 1970. Magnetic reversals and sedimentation rates in the Arctic Basin. *Geol. Soc. Am. Bull.* 81, 3129–3134.
- Clark, D.L., Hansen, A., 1983. Central Arctic Ocean sediment texture: a key to ice-transport mechanism. In: Molnia, B. (Ed.), *Glacial-marine Sedimentation*. Plenum, New York, pp. 301–330.
- Clark, D.L., Whitman, R.R., Morgan, K.A., Mackey, S.D., 1980. Stratigraphy and glacial-marine sediments of the Amerasian Basin, central Arctic Ocean. *Geol. Soc. Am. Spec. Pap.* 181, 1–57.
- Denton, G.H., Hughes, T.J., 1981. The Arctic ice sheet; an outrageous hypothesis. *The Last Great Ice Sheets*. Wiley, New York, NY, USA, pp. 437–467.
- Dyke, A.S., 1999. Last glacial maximum and deglaciation of Devon Island, Arctic Canada: support for an innuitian ice sheet. *Quat. Sci. Rev.* 18, 393–420.
- Ellwood, B.B., 1984. Magnetic fabric and remanence analyses of cores from the U.S. continental margin and the Vema Channel. *Mar. Geol.* 58, 151–164.
- Ellwood, B.B., Ledbetter, M.T., 1979. Paleocurrent indicators in deep-sea sediment. *Science* 203, 1335–1337.
- Evans, J.R., Kaminski, M.A., 1998. Pliocene and Pleistocene chronostratigraphy and paleoenvironment of the central Arctic Ocean, using deep water agglutinated foraminifera. *Micropaleontology* 44, 109–130.
- Flower, B.P., 1997. Overconsolidated section on the Yermak Plateau, Arctic Ocean Ice sheet grounding prior ca 660 ka? *Geology* 25, 147–150.
- Frederichs, T., 1995. Regional and temporal variations of rock magnetic parameters in Arctic marine sediments. *Ber. Polarforschung* 164, 1–212.
- Fütterer, D.K., 1992. ARCTIC '91: The expedition ARK VIII/3 of RV Polarstern in 1991. *Ber. Polarforschung*, 107.
- Gard, G., 1993. Late quaternary coccoliths at the North Pole: evidence of ice-free conditions and rapid sedimentation in the central Arctic Ocean. *Geology* 21, 227–230.
- Gard, G., Backman, J., 1990. Synthesis of Arctic and sub-Arctic coccolith biochronology and history of North Atlantic drift water influx during the last 500,000 years. In: Bleil, U., Thiede, J. (Eds.), *Geological History of the Polar Oceans: Arctic versus Antarctic*. NATO ASI Ser. C, vol. 308, pp. 417–436.
- Grosswald, M.G., 1980. Late Weichselian ice sheets of northern Eurasia. *Quat. Res.* 13, 1–32.
- Haq, B.U., Lohmann, G.P., 1976. Early Cenozoic calcareous nannoplankton biogeography of the Atlantic Ocean. *Mar. Micropaleontol.* 1, 119–194.
- Hughes, T.J., Denton, G.H., Grosswald, M.G., 1977. Was there a late Würm ice sheet? *Nature* 266, 596–602.
- Ishman, S.E., Polyak, L., Poore, R.Z., 1996. An expanded record of pleistocene deep arctic change: Canada Basin, western Arctic Ocean. *Geology* 24, 139–142.
- Jakobsson, M., 1999. First high-resolution chirp sonar profiles from the central Arctic Ocean reveal erosion of Lomonosov Ridge sediments. *Mar. Geol.* 158, 111–123.
- Jakobsson, M., Løvlie, R., Al-Hanbali, H., Arnold, E., Backman, J., Mörth, M., 2000. Manganese and color cycles in Arctic Ocean sediments constrain Pleistocene chronology. *Geology* 28, 23–26.
- Jokat, W., Uenzelmann-Neben, G., Kristoffersen, Y., Rasmussen, T.M., 1992. Lomonosov Ridge—A double-sided continental margin. *Geology* 20, 887–890.
- Jokat, W., Weigelt, E., Kristoffersen, Y., Rasmussen, T.M., Schöne, T., 1995. New insights into the evolution of the Lomonosov Ridge and the Eurasian Basin. *Geophys. J. Int.* 122, 378–392.
- Jones, R.L., Whatley, R.C., Cronin, T.M., Dowsett, H.J., 1999. Reconstructing late Quaternary deep-water masses in the eastern Arctic Ocean using benthonic Ostracoda. *Mar. Micropaleontol.* 37, 251–272.
- Karlén, W., Lundqvist, J., Rutter, N.W., Teller, J.T., Catto, N.R. (Eds.), 1998. Problematic Ice Sheets. *Quat. Int.*, vol. 45/46, pp. 1–142.
- Lagoe, M.B., 1977. Recent benthic foraminifera from the central Arctic Ocean. *J. Foraminiferal Res.* 7, 106–129.
- Larsen, E., Funder, S., Thiede, J., 1999. Late Quaternary history of northern Russia and adjacent shelves—synopsis. *Boreas* 28, 6–11.
- Løvlie, R., Markussen, B., Sejrup, H.P., Thiede, J., 1986. Magnetostratigraphy in three Arctic Ocean sediment cores; arguments for magnetic excursions within oxygen-isotope stage 2–3. *Phys. Earth Planet. Int.* 43, 173–184.
- Mayer, L.A., 1979. The origin of the fine scale acoustic stratigraphy in deep sea carbonates. *J. Geophys. Res.* 84 (B11), 6177–6184.
- Morris, T.H., Clark, D.L., Blasco, S.M., 1985. Sediments of the

- Lomonosov Ridge and Markov Basin: a Pleistocene stratigraphy for the North Pole. *Geology* 96, 901–910.
- Myhre, A.M., Thiede, J., Firth, J.V. et al., 1995. Proc. Ocean Drill. Prog. (Initial reports), 151, College Station, Texas, Ocean Drilling Program, 1-926.
- Nowaczyk, N.R., Baumann, M., 1992. Combined high-resolution magnetostratigraphy and nannofossil biostratigraphy for late Quaternary Arctic Ocean sediments. *Deep-Sea Res.* 39, 567–601.
- O'Neill, B.J., 1981. Pliocene and Pleistocene benthic foraminifera from the central Arctic Ocean. *J. Paleontol.* 55, 1141–1170.
- Phillips, R.L., Grantz, A., 1997. Quaternary history of sea ice and paleoclimate in the Amerasia basin, Arctic Ocean, as recorded in cyclical strata of Northwind Ridge. *Geol. Soc. Am. Bull.* 109, 1101–1115.
- Polyak, L.V., 1986. New data on microfauna and stratigraphy of bottom sediments of the Mendeleev Ridge, Arctic Ocean. In: Andreev, S.I. (Ed.), *Sedimentogenesis and Nodule-Formation in the Ocean*. Sevmorgeologia, Leningrad, pp. 40–50 (in Russian).
- Polyak, L.V., 1990. General trends of benthic foraminiferal distribution in the Arctic Ocean. In: Kotlyakov, V.M., Sokolov, V.E. (Eds.), *Arctic Research: Advances and Prospects*. Part 2. Nauka, Moscow, pp. 11–213.
- Polyak, L., Forman, S.L., Herlihy, F.A., Ivanov, G., Krinitsky, P., 1997. Late Weichselian deglacial history of the Svyataya (Saint) Anna Trough, northern Kara Sea, Arctic Russia. *Mar. Geol.* 143, 169–188.
- Polyak, L., Edwards, M.H., Coakley, B.J., Jakobsson, M., 2001. Ice shelves in the Pleistocene Arctic Ocean inferred from glaciogenic deep-sea bedforms. *Nature* 410, 453–457.
- Poore, R.Z., Ishman, S.E., Phillips, L., McNeil, D., 1994. Quaternary stratigraphy and paleoceanography of the Canada Basin, Western Arctic Ocean. *U.S. Geol. Surv. Bull.* 2080, 1–32.
- Schock, S.G., LeBlanc, L.R., Mayer, L.A., 1989. Chirp subbottom profiler for quantitative sediment analysis. *Geophysics* 54, 445–450.
- Scott, D.B., Mudie, P.J., Baki, V., MacKinnon, K.D., Cole, F.E., 1989. Biostratigraphy and late Cenozoic paleoceanography of the Arctic Ocean: foraminiferal, lithostratigraphic, and isotopic evidence. *Geol. Soc. Am. Bull.* 101, 260–277.
- Sejrup, H.P., Gifford, H.M., Brigham-Grette, J., Løvlie, R., Hopkins, D., 1984. Amino acid epimerization implies rapid sedimentation rates in Arctic ocean cores. *Nature* 310, 772–775.
- Spielhagen, R.F., Bonani, G., Eisenhauer, A., Frank, M., Frederichs, T., Kassens, H., Kubik, P.W., Mangini, A., Norgaard-Pedersen, N., Nowaczyk, N.R., Schper, S., Stein, R., Thiede, J., Tiedemann, R., Wahsner, M., 1997. Arctic Ocean evidence for late Quaternary initiation of northern Eurasian ice sheets. *Geology* 25, 783–786.
- Stein, R. (Ed.), 1998. Arctic Paleo-River Discharge (APARD)—A New Research Program of the Arctic Ocean Science Board (AOSB). Reports on Polar Research 279. Alfred Wegener Institute, Bremerhaven, pp. 1–127.
- Stein, R., Korolev, S., 1994. Shelf-to-basin sediment transport in the eastern Arctic Ocean. In: Kassens, H., Hubberten, H.-W., Pryamikov, S.M., Stein, R. (Eds.), *Russian–German Cooperation in the Siberian Shelf Seas: Geo-System Laptev Sea*. Reports on Polar Research 144. Alfred Wegener Institute, Bremerhaven, pp. 87–100.
- Stein, R., Grobe, H., Washner, M., 1994a. Organic carbon, carbonate, and clay mineral distributions in eastern central Arctic Ocean surface sediments. *Mar. Geol.* 104, 269–285.
- Stein, R., Schubert, C., Vogt, C., Fütterer, D.K., 1994b. Stable isotope stratigraphy, sedimentation rates, and salinity changes in the Latest Pleistocene to Holocene eastern central Arctic Ocean. *Mar. Geol.* 119, 333–355.
- Steuerwald, B.A., Clark, D.L., Andrew, J.A., 1968. Magnetic stratigraphy and faunal patterns in Arctic Ocean sediments. *Earth Planet. Sci. Lett.* 5, 79–85.
- Tarling, D.H., Hrouda, F., 1993. *The Magnetic Anisotropy of Rocks*. Chapman & Hall, London.
- Thiede, J., Bauch, H.A., 1999. The Late Quaternary history of northern Eurasia and the adjacent Arctic Ocean: an introduction to QUEEN. *Boreas* 28, 3–5.
- Thierstein, H.R., Geitzenauer, K.R., Molfino, B., Shackleton, N.J., 1977. Global synchronicity of late Quaternary coccolith datum levels: validation by oxygen isotopes. *Geology* 5, 400–404.
- Thompson, R., Oldfield, F., 1986. *Environmental Magnetism*. Allen & Unwin, London, 227 pp.
- Vogt, P.R., Crane, K., Sundvor, E., 1994. Deep Pleistocene iceberg plowmarks on the Yermak Plateau: sidescan and 3.5 kHz evidence for thick calving ice fronts and a possible marine ice sheet in the Arctic Ocean. *Geology* 22 (5), 403–406.
- Washner, M., Müller, C., Stein, R., Ivanov, G., Levitan, M., Shelekova, E., Tarasov, G., 1999. Clay-mineral distribution in surface sediments of the Eurasian Arctic Ocean and continental margin as indicator for source areas and transport pathways—a synthesis. *Boreas* 28, 215–232.
- Weeks, R., Laj, C., Endignoux, L., Fuller, M., Roberts, A., Manganne, R., Blanchard, E., Goree, W., 1993. Improvements in long-core measurement techniques: applications in paleomagnetism and paleoceanography. *Geophys. J. Int.* 114, 651–662.